

Hierarchical Control of a park of floating Oscillating Water Column Wave Energy Converters

Daniel T. Gaebele and Mario E. Magaña

Abstract—Ocean wave energy is a renewable energy which remains costly for large-scale electricity generation. The oscillating water column (OWC) is a wave energy converter (WEC) device-type with a rectifying air turbine and generator which convert alternating airflow induced by the water motion into kinetic energy then to electric energy. Although the OWC is a promising device-type, there are still several challenges to overcome to achieve commercial energy production. Capital cost, of which mooring lines and power transmission cables contribute significantly, is one major challenge. To reduce this cost, developers can deploy multiple devices close to each other in WEC parks. Applying control at each stage of energy conversion to increase the electric energy output of the devices and ensure a safe operation, can reduce the levelized cost of energy and cost associated with maintenance. Herein, we first present a statespace model of a park of seven hydrodynamically interacting floating OWCs in all degrees of freedom with nonlinear PTO dynamics and a shared, quasistatic mooring model. The electric power flow is modeled by considering the conversion losses from the AC generators over a DC link, including a storage unit to the grid connection. Secondly, we express the OWC park from a higher hierarchical level as an automaton driven by discrete events. Finally, we use a standard supervisory control approach to enable different local control schemes to ensure a safe operation of the individual WEC and the park and to improve the efficiency of the electromagnetic energy conversion. The supervisor has good adaptability potential for different WECs and the incorporation of safety mechanisms.

Index Terms—Array, Automaton, Discrete Event, Floating Oscillating Water Column, Hierarchical Control, Wave to Wire Model.

I. Introduction

AVE energy converter (WEC) researchers and developers continue to work to improve the viability of the technology as a source

This paragraph of the first footnote will contain the ID number of your paper submission and the conference track where the paper was submitted. The work was sponsored by the National Science Foundation, USA (Award Number: 1711859).

D. Gaebele and M. Magaña are with the Department of Electrical and Computer Engineering, Oregon State University, Corvallis, OR, 97331 USA. e-mail: (gaebeled@oregonstate.edu, magana@eecs.oregonstate.edu).

of near-zero emission electricity. Recently, support for work in wave energy technology development for non-grid-scale applications has increased due to the many pressing challenges presented by climate change, including water shortages, ocean acidification, and rising sea levels. Emerging market wave energy applications are also attractive as a stepping stone toward girdscale deployment, the costs and risk of which still remain too high. In addition to new pathways, wave energy researchers continue to find ways to drive down costs, improve performance, and ensure safety, reliability, and acceptability of grid-scale devices. Control design has long been and continues to be one of the primary areas of research for reaching those goals [1]. The purpose of the control algorithms is almost always to maximize energy absorption from the incoming waves, subject to the WEC dynamics and the physical limitations of the device and the actuators [2]. Recently, there has been a drive to reduce algorithm complexity by, for example, avoiding excitation force estimation or forecasting and circumventing online numerical optimization, both of which require complex computations by the controller at every time step [3]. Another challenge for control arises when the wave resource exceeds the rated device power. In wind turbines, this is dealt with by blade pitch control to the shed power [4]. For WECs shedding strategies would be strongly dependent on the archetype [3]. One type of WEC where such strategies are possible is the oscillating water column (OWC) WEC. The OWC can shed power by closing an additional valve, called the high speed stop valve (HSSV) [5]. But, there is minimal research in WEC control that addresses multiple control challenges at once, such as shedding power at some times, while maximizing power at other times.

The OWCs are a promising device-type because of their simplicity. Under normal operation, the power take off (PTO) does not come in contact with water. Instead, the rectifying air turbine and the water column enclose an air chamber. The turbine and (typically) a directly connected

1

generator convert the alternating airflow induced by the water motion into kinetic energy, then to electric energy. Although, there is potential for low-power single OWC applications [6], floating point-absorber type OWCs are also a great candidate to deploy in parks. For grid-scale electricity production, parks of WECs seem more viable compared to single huge device due to benefits like modularity and deployability, and the ability to share mooring systems, thereby reducing the high cost for bottom mooring lines [7]. We design our control schemes based on a case study of data publicly available of the IDOM Marmok A-5 spar-buoy OWC [8]. This floating OWC has been successfully deployed for three years at the BiMEP test site (Basque Country, Spain) within the H2020 OPERA Project (http://opera-h2020.eu/). We select the biradial turbine for this work and assume an HSSV is installed in front of the turbine [9]. We assume a WEC park of seven devices placed in an equilateral hexagon with one WEC in the center, as first suggested by Vicente et al. [10]. We will call the equilateral triangle array, which is oriented off shore (negative surge axis in Fig. 1) the server array and the 4 WECs surrounding the center WEC, with $x \geq 0$, the clients when it comes to reference following. The server array has the benefit that it can pass on information about the incoming waves to the client WECs without the need for wave prediction [4].

In this paper, we first develop a detailed floating OWC park simulation model in state space form. Then, we describe the WEC park as a discrete event system. Last, we design a supervisory controller that sits on a higher hierarchical level than the local controllers governing the energy conversion. We follow the standard supervisory control approach previously used for the control of wind power systems [11]. The control design is based on the knowledge of the two proceeding models. The supervisor will automatically enable and disable local controllers based on the current operating regime. Other hierarchical control approaches for WECs are focused on reducing the sensitivity to modelling errors while maximizing energy conversion [12], or for reference generation [13]. We want to achieve a more holistic approach, trying to efficiently convert energy in all kinds of operating regions and shedding power when necessary.

II. MODELLING

The main purpose for the state space model of the entire OWC park is to simulate the WEC response in the time domain. The physical meaning of the state space states is helpful for determining the discrete states when looking at the park from a higher level for the discrete event model in Sec. II-E. To describe the current state of the WEC park, we start with the position vector

$$\boldsymbol{x}_{\mathrm{pos},i} = \begin{bmatrix} x_i & y_i & z_i & r_i^x & r_i^y & r_i^z & z_i^p \end{bmatrix}^T,$$
 (1)

which contains the displacements x_i (surge), y_i (sway), z_i (heave) and the rotations about the respective axis r_i^x (roll), r_i^y (pitch), r_i^z (yaw) expressed in a inertial (world-fixed) coordinate frame for WEC i. The last entry in (1) is the heave position of the imaginary piston representing the water column inside the WEC z_i^p . To express the dynamics of a WEC, a body-fixed reference frame should be used, since the inertial properties of the WEC remain constant in time in this frame [14]. We use the linear mapping $J_{r,i}$ at every time step to correct for the translations and rotations between body frame ($\hat{}$) and world frame, namely

$$\boldsymbol{x}_{\text{vel},i} = \boldsymbol{J}_{r,i} \underbrace{\left[\dot{\hat{x}}_{i} \quad \dot{\hat{y}}_{i} \quad \dot{\hat{z}}_{i} \quad \dot{\hat{r}}_{i}^{x} \quad \dot{\hat{r}}_{i}^{y} \quad \dot{\hat{r}}_{i}^{z} \quad \dot{\hat{z}}_{i}^{p} \right]^{T}}_{\hat{\boldsymbol{x}}_{\text{vel},i}} \qquad (2)$$
with,
$$\boldsymbol{J}_{r,i} = \begin{bmatrix} \boldsymbol{R}_{r,i} & \boldsymbol{0}^{3 \times 3} & \boldsymbol{0} \\ \boldsymbol{0}^{3 \times 3} & \boldsymbol{T}_{r,i} & \boldsymbol{0} \\ \boldsymbol{0}^{1 \times 3} & \boldsymbol{0}^{1 \times 3} & \cos r_{i}^{y} \cos r_{i}^{x} \end{bmatrix}.$$
(3)

Here $R_{r,i}$ the intrinsic rotation matrix about r_i^z , r_i^x , r_i^y is applied to the transnational velocities. The rotation,

$$\boldsymbol{T}_{r,i} = \begin{bmatrix} 1 & \sin r_i^x \tan r_i^y & \cos r_i^x \tan r_i^y \\ 0 & \cos r_i^x & -\sin r_i^x \\ 0 & \sin r_i^x / \cos r_i^y & \cos r_i^x / \cos r_i^y \end{bmatrix}$$
(4)

is applied to the rotational velocities [14]. The last entry of (3) governs the pistons heave velocity inside the potentially rotated WEC.

A. Wave Body Interactions

The hydrodynamic model of the WEC park is based on linear water wave theory and described in more detail in our prior work [15]. In order to extend our case study from an array of three devices to the WEC park with seven devices we had to remove the imaginary water column representation in the boundary element solver, ANSYS Aqwa, to obey the mesh elements constraints. As part of the post-processing, we combine the hydrodynamic coefficients in all six degrees of freedom (DoF) of the seven buoys with the heave characteristics of the imaginary full water columns previously identified [15]. A detailed study on the combination exceeds the scope of this paper. We make practical corrections with nonlinear forces to mitigate the limitations of the linear approach, such as the viscous drag force, mooring force and the nonlinear force connecting

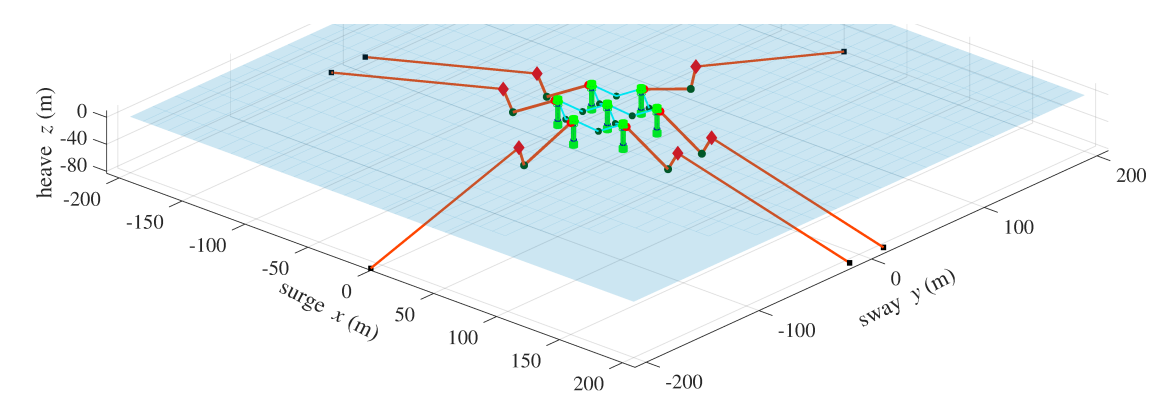


Fig. 1. WEC park and mooring configuration at calm sea. The heave axis aspect ratio is not equal to the surge and sway axis.

the buoy and it's water column due to the air pressure inside the chamber. Now, taking into account that the forces act along the time varying body axes, we can formulate Cummins equation in our notation,

$$\dot{\hat{\boldsymbol{x}}}_{\text{vel},i} = \boldsymbol{M}_{i}^{-1} \left(\boldsymbol{F}_{i}^{\text{H}} + \boldsymbol{F}_{i}^{\text{M}} + \boldsymbol{F}_{i}^{\text{PTO}} + \boldsymbol{F}_{i}^{\text{R'}} + \boldsymbol{F}_{i}^{\text{Ex}} + \boldsymbol{F}_{i}^{\text{VD}} \right). \tag{5}$$

Here \boldsymbol{M}_i^{-1} denotes the inertia matrix, containing the added mass and body i to body i interactions. The considered generalized forces vectors \boldsymbol{F}_i on WEC i are composed out a linear force vector and rotational torque vector.

 $F^{\rm H}$ The hydrostatic restoring force vector (Following Oikonomou et al. [16]).

F^M The mooring force vector due to mooring connection with the sea floor and the inter body moorings (Sec.II-A1). No mooring is connected to the imaginary piston.

F^{Ex} The excitation force vector accounts for all incident waves on the body. The extension to six DoF is trivial if the hydrodynamic excitation force coefficients are available [17].

F^R The radiation force vector, including interactions with the motion of other bodies in the park. Results from solving the radiation problem, approximated with a linear state space model. We neglect many radiation interactions between spatially distinct WECs, if the magnitude off the radiation impulse response function is below a somewhat arbitrary threshold.

F^{PTO} The force vector due to the pressure change in the chamber induced by the turbine/generator dynamics. Acting in opposite direction for buoy and OWC (Sec. II-B).

 $F^{
m VD}$ The viscous drag force vector based on the common assumption of a constant drag coefficient following the semi-empirical Morison equation.

Giorgi et al. model with more hydrodynamic detail, e.g. nonlinear Froude-Krylov and Coriolis force and consequently are able to detect parametric resonance [14]. In the model that we present, we did not observe parametric resonance, although the respective degrees of freedom are coupled. However, note that our focus is on our control-oriented notation of the dynamics and not detailed nonlinear hydrodynamics.

1) Mooring Model: In this work we use a quasistatic mooring model. A quasi-static model can capture some of the nonlinear mooring behavior, but neglects the line motion itself [18]. Giorgi et al. present a compact description of the nonlinear equations to model a bottom mooring line [14]. Such a mooring line is illustrated in Fig 1 in orange. The line is composed of three straight lines, with lengths L_1, L_2, L_3 and a jumper (diamond) and clump weight (circle) in between. We use this type of mooring for the bottom mooring lines, due to its capability to station keep without significantly limiting the heave motion [19]. For simplicity, the mooring line is projected in a plane cutting through the anchor on the sea floor (square) and the buoy, so that we can use the horizontal distance h(t) and the vertical distance z(t) to numerically compute the tension of the cable at the buoy T_b and the anker T_a . We restate the slightly recasted equation system [14], with the vertical and horizontal force balance

$$0 = T_{b} \sin \alpha_{3} - w_{L}(L_{1} + L_{2} + L_{3})$$

$$- F_{C} + F_{J} - T_{a} \cos \alpha_{1}$$

$$0 = T_{b} \cos \alpha_{3} - T_{a} \cos \alpha_{1}.$$
(6)
(7)

Followed by a torque balance,

$$0 = T_{b} \cos \alpha_{3} z(t) - T_{b} \sin \alpha_{3} h(t)$$

$$+ w_{L} \left[\cos \alpha_{1} \left(\frac{L_{1}^{2}}{2} + L_{1} L_{2} + L_{2} L_{3} \right) + \cos \alpha_{2} \left(\frac{L_{2}^{2}}{2} + L_{2} L_{3} \right) + \cos \alpha_{3} \frac{L_{3}^{2}}{2} \right]$$

$$+ \cos \alpha_{1} L_{1} \left(F_{C} - F_{I} \right) + \cos \alpha_{2} F_{C},$$

$$(8)$$

and lastly two equations imposing geometrical constraints,

$$0 = \cos \alpha_1 L_1 + \cos \alpha_2 L_2 + \cos \alpha_3 L_3 - h(t)$$
 (9)

$$0 = \sin \alpha_1 L_1 + \sin \alpha_2 L_2 + \sin \alpha_3 L_3 - z(t). \quad (10)$$

Here the unknowns $\alpha_1,\alpha_2,\alpha_3$ denote the angle between the respective line L_1,L_2,L_3 and the horizontal plane. The weight force and buoyancy force of the clump weight and the jumper are denoted $F_{\rm C}$ and $F_{\rm J}$ respectively. In the time domain simulation, we only solve the system eqs. (6) to (10) every 0.1s to and hold the value to save computation time. We use the previous solution as initial guess for the nonlinear equation solver to further decrease the computation time. For the inter body (IB) mooring lines, we assume two lines with length $L_{\rm IB}$ and weight per unit length $w_{\rm IB}$ and a single weight force $F_{\rm IB}$ between a buoybuoy connection. The vertical force and torque balance,

$$0 = -T_{IB_1} \sin \alpha_{IB_1} - 2w_{IB}L_{IB} - F_{C,IB} + T_{IB_2} \sin \alpha_{IB_2}$$
(11)

$$0 = -w_{\rm IB} \frac{L_{\rm IB}^2}{2} (3\cos\alpha_{\rm IB_1} + \cos\alpha_{\rm IB_2}) - F_{\rm C,IB}\cos\alpha_{\rm IB_1} + T_{\rm IB_2} (\sin\alpha_{\rm IB_2} h_{\rm IB}(t) - \cos\alpha_{\rm IB_2} z_{\rm IB}(t))$$
(12)

are a function of the horizontal and vertical distance between two IB moored buoys $h_{\rm IB}(t)$ and $z_{\rm IB}(t)$. If we assume that the IB lines do not change their length, we can explicitly solve for the angles to the horizontal $\alpha_{\rm IB_1}, \alpha_{\rm IB_2}$ with trigonometry. Consequently, we calculate the tensions $T_{\rm IB_1}, T_{\rm IB_2}$ at the ends of the IB mooring lines analytically, with

$$\begin{bmatrix} T_{\text{IB}_1} \\ T_{\text{IB}_2} \end{bmatrix} = \begin{bmatrix} -s_{\text{IB}_1} & s_{\text{IB}_2} \\ 0 & s_{\text{IB}_2} h_{\text{IB}}(t) - c_{\text{IB}_2} z_{\text{IB}}(t) \end{bmatrix}^{-1} \cdot \begin{bmatrix} 2w_{\text{IB}} L_{\text{IB}} + F_{\text{C,IB}} \\ w_{\text{IB}} \frac{L_{\text{IB}}^2}{2} (3c_{\text{IB}_1} + c_{\text{IB}_2}) + F_{\text{C,IB}} c_{\text{IB}_1} L_{\text{IB}} \end{bmatrix} .$$
(13)

In (13) we used $s_{IB} = \sin \alpha_{IB}$ and $c_{IB} = \cos \alpha_{IB}$ for brevity. Finally, we compute the mooring force vector $\boldsymbol{F}_i^{\mathrm{M}}$ by mapping the mooring lines tensions into the body fixed reference frame and adding up the force and torque components.

B. Power Take Off Model

We would like to identify the instantaneous relative chamber pressure $x_{p^*,i}(t)$, to quantify the force acting in opposite direction on buoy and internal water column, namely,

$$\boldsymbol{F}_{i}^{\text{PTO}} = p_{\text{at}} S_{\text{OWC}} x_{p^*,i}(t). \tag{14}$$

Here, p_{at} denotes the atmospheric pressure and S_{OWC} the surface of the internal water column.

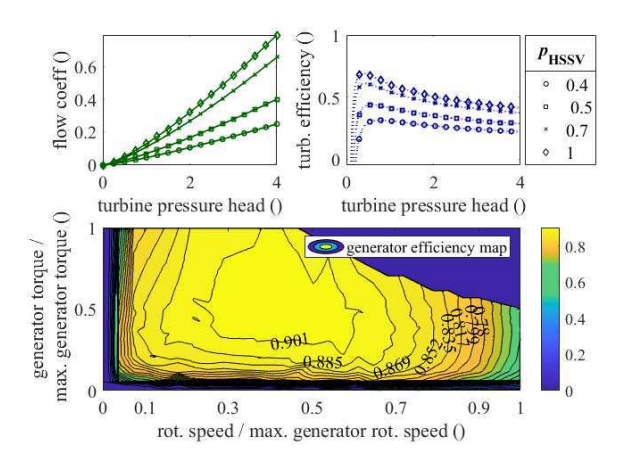


Fig. 2. Top: Dimensionless turbine characteristics as a function of the dimensionless pressure head and the position of the HSSV $p_{\rm HSSV}$. Bottom: Generator efficiency map as a function of the turbine-generator sets rotational speed and generator (control) torque [21].

Air compressibility introduces nonlinearities to the OWC dynamics which are modeled in detail together with the dynamics of the biradial turbine in [9]. Based on a mass balance of the air chamber, assuming that air acts as a perfect gas when expanding and compressing, the change rate of the relative chamber pressure $\dot{x}_{p^*,i}(t)$ results in a function of the instantaneous chamber volume, the change rate of the camber volume and the airflow through the turbine $\dot{m}_{t_i}(t)$. Consequently, the heave position of the buoy and piston and their velocity directly affect the energy contained air chamber,

$$\dot{x}_{p^*,i}(t) = f_{p^*}\bigg(\boldsymbol{x}_{pos}(k), \boldsymbol{x}_{vel}(k), \dot{m}_{t_i}(t)\bigg), \quad (15)$$

with k = 3 + 6(i - 1). To identify $\dot{m}_{t_i}(t)$, we need the turbine/generator set dynamics in terms of angular rotational speed $x_{\Omega,i}(t)$,

$$\dot{x}_{\Omega,i}(t) = \frac{1}{J} \left(T_{\mathsf{turb}_i} - T_{\mathsf{gen}_i} - Bx_{\Omega,i} \right). \tag{16}$$

Here J is the composite moment of inertia (MOI) of the $i^{\rm th}$ turbine/generator set, B is a constant that models viscous friction losses. The instantaneous torque induced by the air pressure of the air flow through the $i^{\rm th}$ turbine $T_{\rm turb_i}$, will be called turbine torque and $T_{\rm gen_i}$ denotes the instantaneous generator torques of the $i^{\rm th}$ WEC. In this work we identify the turbine torque with the experimentally obtained performance characteristics of the biradial turbine, illustrated in Fig. 2, as in [20]. Those characteristics are a function of the dimensionless turbine pressure head, which itself is a function of $x_{\Omega,i}(t)$ and $x_{p^*,i}(t)$, and a function of the position of the HSSV $p_{\rm HSSV}$. We do

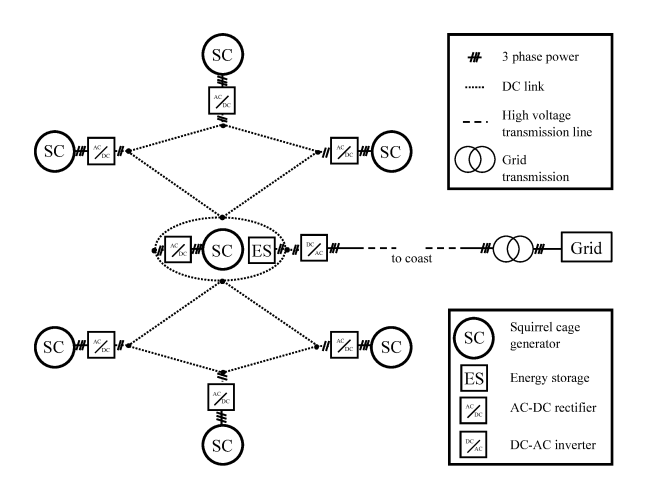


Fig. 3. Electric power flow model of the WEC park.

not model the detailed generator current equations since the generator electromagnetic dynamics are much faster than the system dynamics of the WEC. Instead, we use the empirical data of the generator efficiency $\eta_{\rm gen}$ of a SIEMENS IEC low-voltage electrical generator model 1LE1603-2AB53-4GB4-Z [20], [21], illustrated in Fig. 2. We also assume that the generator is run in torque mode and we always receive $T_{{\rm gen},i}$ commanded by the drive. Now we can state the alternating current (AC) electric power,

$$P_{\text{elec},i}^{\text{AC}} = \eta_{\text{gen},i} | T_{\text{gen},i} | x_{\Omega,i}(t)$$
 (17)

Lastly, let us define the control inputs

$$u_{\text{gen},i} = T_{\text{gen},i}, \text{ and}$$
 (18)

$$u_{\text{HSSV},i} = p_{\text{HSSV},i}, \in [0,1].$$
 (19)

After the electromechanical power conversion of the generator, we draw an artificial system boundary, since the following electric energy conversion dynamics do not interact with the WECs' hydrodynamics.

C. Electric Power Flow Model

The next steps in the power conversion chain happen with much faster dynamics than the WEC motion. Consequently, we do not model the switching dynamics of power electronics (PE). Instead, we work with constant efficiencies to account for power dissipation. The electric components and connections are illustrated in Fig. 3. We assume that every single WEC has the PE to convert from AC to direct current (DC), with round trip efficiency η_{PE} , hence

$$P_{\text{elec},i}^{\text{DC}} = \begin{cases} \eta_{\text{PE}} P_{\text{elec},i}^{\text{AC}}, & \text{for } P_{\text{elec},i}^{\text{AC}} \ge 0\\ P_{\text{elec},i}^{\text{AC}} / \eta_{\text{PE}}, & \text{for } P_{\text{elec},i}^{\text{AC}} < 0. \end{cases}$$
(20)

Next, we model a DC-link so that the power can flow freely between the different WECs in the park. This enables the use of the squirrel cage generator in motor mode, e.g. for reference speed following. The power necessary to turn one WEC's turbine could come from another WEC which is generating at that moment. The high current cables could, for example, go along the IB mooring lines. Furthermore, the DC-link is directly connected to a storage medium and it is connected to the grid via an inverter with efficiency $\eta_{\text{PE,IV}}$, The instantaneous power of the link is therefore,

$$P_{\text{link}} = \sum_{i} P_{\text{elec},i}^{\text{DC}} - P_{\text{load}}$$
 (21)

If the grid load power $P_{\rm load}$ can be met by the aggregated power of the individuals WECs $P_{\rm link} \geq 0$. On the other hand, if the load is not met the differences need to come from the storage medium with efficiency $\eta_{\rm SM}$. We use the state of charge $x_{\rm C}$ of the battery as the last state space state, with it's change rate being

$$\dot{x}_{\rm SOC} = \frac{1}{W_{\rm SM}^{\rm rated}} \begin{cases} \eta_{\rm SM} P_{\rm link}, & \text{for } P_{\rm link} \ge 0 \\ P_{\rm link} / \eta_{\rm SM}, & \text{for } P_{\rm link} < 0. \end{cases}$$
(22)

Here W_{SM} denotes the rated storage capacity of the battery. Since we can assume that the amount of grid power transmission is controllable , we can define the last input,

$$u_{\text{load}} = P_{\text{load}}.$$
 (23)

This finalizes the power conversion chain from wave to wire.

D. OWC Park State Space Simulation Model

We transform the equations above to represent them in the state space with variable vector, i.e.

$$\dot{\boldsymbol{x}} = \begin{bmatrix} \dot{\boldsymbol{\mathcal{X}}}_{\text{pos}} \\ \dot{\boldsymbol{\mathcal{X}}}_{\text{vel}} \\ \dot{\boldsymbol{x}}_{p^*} \\ \dot{\boldsymbol{x}}_{\Omega} \\ \dot{\boldsymbol{x}}_{\text{SOC}} \end{bmatrix} = \begin{bmatrix} \boldsymbol{\mathcal{J}}_r \hat{\boldsymbol{\mathcal{X}}}_{\text{vel}} \\ (\boldsymbol{\mathcal{M}})^{-1} \cdot \boldsymbol{\mathcal{F}}(\boldsymbol{x}) \\ \boldsymbol{f}_{p^*}(\boldsymbol{x}, \boldsymbol{u}_{\text{HSSV}}) \\ \boldsymbol{f}_k(\boldsymbol{x}_{p^*}, \boldsymbol{x}_{\Omega}, \boldsymbol{u}_{\text{gen}}) \\ \boldsymbol{f}_{\text{SM}}(\boldsymbol{x}_{\Omega}, \boldsymbol{u}_{\text{gen}}, u_{\text{load}}) \end{bmatrix}$$
(24)

Note that script letters represent concatenated vectors and matrices to include all vectors $i \in [1;7]$. The inertial matrix $(\mathcal{M})^{-1}$ contains entries connecting spatially distinct WECs due to the added mass components. Further cross body interacions originate from the mooring force and the radiation force, hidden in $\mathcal{F}(x)$. The pressure, rotational speed and charge states change rates in (24) are presented as functions of their major drivers, but follow eqs. (15), (16) and (22) respectively.

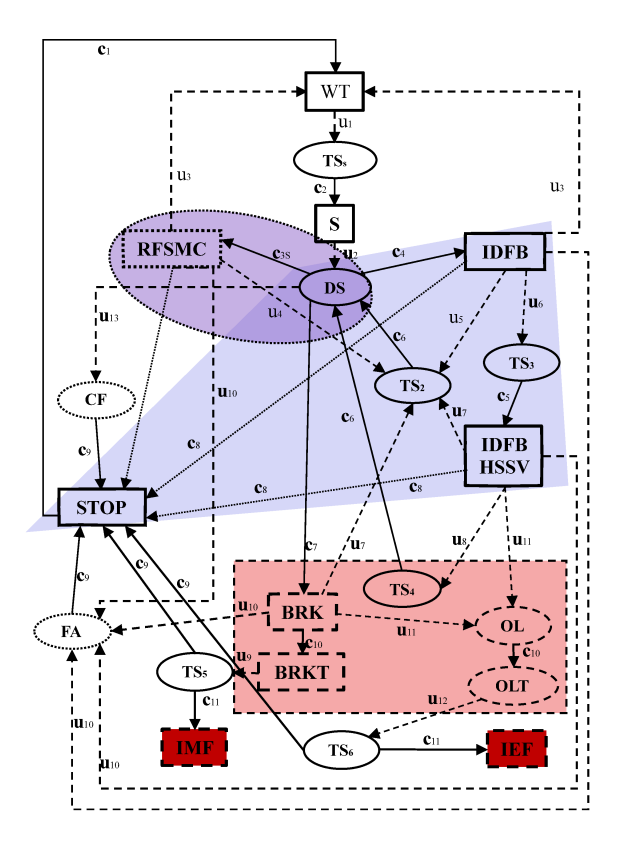


Fig. 4. Discrete event model of the WEC park G.

E. Discrete Event Model OWC Park

A supervisory control based on the concept of discrete-event systems (DES) naturally yields a hierarchical structure. Each level of control causes an allowable range of operation for the lower levels [22]. The DES itself evolves with the occurrence of events [23]. One example type of event would be if the generator exceeds its maximal admissible rotational speed. When looking at the state space time domain simulation model from this perspective, the continuous dynamics between events are unimportant. The discrete states from the set Q of a DES should not be confused with state space states with a clear physical meaning. The discrete states describe an operating regime of the WEC. The possible paths of discrete states via events is illustrated in Fig. 4 for the entire (controlled) WEC park.

1) OWC Park Automaton: The Automaton G_i describes the discrete event dynamics of the WEC i in the WEC park. Herein, we extend G from the work of Bratcu et al., who model the behaviour of a wind turbine for safe and optimal operation [11]. Note that the Automaton in Fig. 4 is vectorized, i.e. bold face indicates a vector of states or events with each entry accounting for a single WEC. Clearly, different WECs can be in different states at the same instance of time. A few uncontrollable events, namely u_1 , u_2 and u_4 are effective globally. The controllable event

 c_{3S} can only be activated for the WECs in the client part of the array, thus the state RFSMC can only be reached by such, since the server array determines the reference velocity. The functional states are all indicated by the box around them, and we identify the following states to describe the possible behavior of an OWC.

WT Waiting
S Start

RFSMC Reference following with SMC
IDFB Ideal Feedback control
IDFB HSSV Ideal FB control with HSSV
BRK Break sequence
BRKT Break sequence timer
STOP Stop park

IMF Irreversible mechanical failure IEF Irreversible electrical failure

Note that discrete states such as vibrations or parametric resonance could be easily included in the Automaton, but since our time domain model is not capable of simulating such effects, we neglect them. The states contained in the blue trapezoid and the purple ellipsoid represent the desired behavior of the system and will be referred to as marked states $Q_{m,i}$. The marked states $Q_{\mathrm{m},i} \subset Q_i$ model a cyclic working process and all but the STOP state are the functional states responsible for power conversion. The STOP state needs to be accessible from all other states, in case of a manual shut down of the WEC, through the controllable event $c_{8,i}$. A safe operation of the automaton is achieved if the catastrophic state IRF and IEF are prevented. We define the desired states $Q_{D,i} = Q_i - \{IRF_i, IEF_i\}.$ The states inside the red rectangle are states of extreme operation and are only admissible for a limited amount of time, thus the corresponding timing states. The overload state OL is not a functional state, in the sense that no controller can prevent electrical overload once it occurs (all local controllers have protection mechanisms included to avoid overload, so if OL is reached, the local controller failed).

We introduce transition states to model the time for decision making of the supervisor (here one time step) and to break algebraic loops, since e.g. the position of the stop valve is used to determine a discrete state, but is also a control output at the same time. Therefore, we use the temporary states:

DS Decision state

CF Control failure

FA Failure

TS Transition states

OL Overload state

The events that the actuators in the WEC can control are called controllable events $\Sigma_{c,i}$:

c₁ WEC activation

- c₂ Start power conversion
- c₃ Enable reference following control (SMC)
- c₄ Enable Ideal Feedback (FB) control
- c₅ Enable FB and HSSV control
- c₆ Disable current controller
- c₇ Enable break sequence
- c₈ Manual stop / c₉ Emergency stop
- c_{10} Start counting / c_{11} Continue counting

The behaviour of the discrete model is complete with the uncontrollable events $\Sigma_{\mathbf{u},i}$:

- u₁ Enough WEC heave motion (global)
- u₂ Turbine rotation > min. generator speed
- u₃ Not enough WEC heave motion (global)
- u₄ Medium-High WEC heave motion (global)
- u₅ Low WEC heave motion (global)
- u₆ Turbine at 90% max. generator speed
- u₇ Turbine below 90% max. generator speed
- u₈ Turbine over max. speed
- u₉ Half of time over max. speed passed
- u₁₀ Functional failure
- u₁₁ Half of admissible time in overload passed
- u₁₂ No suitable controller found

This yields the set of all events $\Sigma_i = \Sigma_{\mathrm{c},i} \cup \Sigma_{\mathrm{u},i}$. To describe the transition between the states in Q_i via the events in Σ_i , the transition function $\delta_i: Q_i \times \Sigma_i \to Q_i$ is commonly used. Note that the event c_{3S} is blocked for the server array. Uncontrollable events are always able to occur. This fully describes the automaton for each WEC

$$G_i = (Q_i, \Sigma_i, \delta_i, q_0, Q_{m,i}), \tag{25}$$

with the initial state q_0 being the STOP state for the entire park.

2) Global Array State: We model the global array state based on a the server array motion, the failure state of the WECs and the current state of charge to determine the amount of power that should go to the grid transmission. The resulting Automaton is trivial, with the functional states baseload BL, over/under base load, and STOP. We do not present the Automaton and supervisor, because of the multiple ways to define the grid load, e.g. with a simple Fuzzy Logic.

III. CONTROL DESIGN

In this work the controllers only take into account the dominant dynamics. Therefore, we neglect both the much faster current dynamics of the electromagnetic energy conversion and the switching dynamics of the power electronics.

A. Low Level Controllers

First we briefly introduce the local controllers for the park's main purpose, power production, followed by control algorithms for protection and power shedding. 1) Turbine/Generator Control: Henriques et. al. present an ideal feedback relation for the generator control torque based on the instantaneous turbine rotational speed [9], [24], namely,

$$u_{\mathrm{gen},i} = \min\left(a_{\mathrm{bep}}x_{\Omega,i}^2, \, P_{\mathrm{gen}}^{\mathrm{rated}}/x_{\Omega,i}, \, T_{\mathrm{gen}}^{\mathrm{max}}\right).$$
 (26)

It is ideal in terms of the maximization of the aerodynamic efficiency of a fixed OWC which runs the identical biradial turbine and is limited by the physical generator constraints, namely the rated power $P_{\rm gen}^{\rm rated}$ and the maximal generator torque $T_{\rm gen}^{\rm max}$. The parameter $a_{\rm bep}$ is analytically determined from the turbine power characteristics at the best efficiency point [24]. This generator control will function as a benchmark in the time domain simulation.

2) Turbine Reference Speed Following: In [17] we show that the benefits of Sliding Mode Control in terms of power improvements mostly occur in low energetic sea states and need an appropriate reference velocity for the potential available wave energy. Due to the randomness of ocean waves, low energetic responses of WECs occur in the order of minutes due to changing sets of waves, even in high energetic sea states. Therefore, the idea pursued in this work is to detect areas of low WEC response and switch from (26) to a 2nd order SMC control law for reference following [17], namely,

 $u_{\rm gen.}$

$$= T_{\text{gen}}^{\text{max}} \int \begin{cases} -u_i dt, & \text{if } |u_i| > c_{\text{sw},i} \\ -\alpha \operatorname{sgn}(\dot{\sigma_i} - g(\sigma_i)) dt & \text{if } |u_i| \leq c_{\text{sw},i}. \end{cases}$$
(27)

Here σ denotes the switching surface, which is the error to the reference velocity and $g(\sigma_i) = -\lambda \operatorname{sgn} \sigma_i |\sigma_i|^{\gamma}$ ensures convergence to the sliding surface when the gains are chosen properly [25]. We consider the physical constraints with,

$$c_{\text{sw},i} = \min\left(1, P_{\text{rated}}^{\text{gen}}/(T_{\text{gen}}^{\text{max}} x_{\Omega,i})\right).$$
 (28)

The reference speed comes from the server array, which will continue to be controlled with (26). We use a primitive wave estimator, based on the knowledge of incidents of free surface peaks of the three WECs in the server array. Over time, this give us an estimated incident wave angle $\theta_{\rm est}$ and a group velocity $v_{\rm est}$. The reference speed generator negatively offsets and time delays the instantaneous rotational speed of the first two server WECs based on $\theta_{\rm est}$ and $v_{\rm est}$ for the corresponding client WEC, to obtain a low pass filtered reference speed signal.

3) Stop Valve Position Control: The HSSV can limit or cut off airflow through the turbine and consequently reduce conversion between pneumatic

and mechanical power. This power shedding is useful in times, when the mechanical power would exceed the generator constraints. Previously, the HSSV is closed entirely when Ω_{gen}^{max} is reached [24]. But, the generator efficiency map in Fig. 2 indicates that the efficiency $\eta_{\rm gen}$ is dropping significantly beyond $0.9\,\Omega_{\rm gen}^{\rm max}$. Therefore, the HSSV control used here limits the mechanical power by partially closing the HSSV, which is physically possible between 0.4 (60% closed) and 1 (open), for an efficient electro-mechanical conversion. A closure > 0 and < 0.4 is physically not possible since the pressure due to the restricted cross-area is too low for the HSSV to maintain it's position, thus the HSSV would need to be closed entirely. When the HSSV position control is activated we use a straight forward PID controller with anti wind-up structure to maintain $0.9\,\Omega_{\rm gen}^{\rm max}$, when possible within the HSSV constraints.

B. Supervisory Controller

We follow the standard supervisory control approach [22] to constrain the behavior of the previously presented Automaton, combined with some elements presented for the work on wind turbines [11]. The supervisory controller ensures a safe operation of the individual WEC and the WEC park by enabling the different local control schemes. Furthermore, the supervisor aims to improve the efficiency of the electromagnetic energy conversion for the client array, by enabling (27) in times of low WEC response. Ultimately, the supervisor S_i is a discrete event Automaton T_i , driven by the states of the WEC park G_i , with an output map ϕ_i , that imposes a certain behavior onto G_i through a control action γ_i . We name the desired Automaton

$$D_i = (Q_{\mathrm{D},i}, \Sigma_i, \delta_i, q_0, Q_{\mathrm{m},i}). \tag{29}$$

A language of an Automation is the (infinite) set of sequences of events along its path (see paths in Fig. 4). We denote the general language of G_i as $L(G_i)$ and the language of the behaviour over the marked states $L_{\rm m}(G_i)$. The language through the marker states $Q_{\rm m}$, controlled by S_i in G_i is

$$L_{\rm m}(G_i, S_i) = L_{\rm m}(G_i) \cap L(G_i, S_i).$$
 (30)

This is the desired closed loop language.

1) Controllability And Supervisor Formal Design: Now, let the language of the desired behavior of Automaton D_i be denoted K_i . Generally, the aim of the supervisor is not to modify $L(G_i)$ itself, but to achieve the desired language $L_{\rm m}(G_i,S_i)$, while maintaining the nonblocking behaviour. The necessary conditions for this language controllability [[22], prop. 4.1] are restated in

Continuous	Discrete state
rot. speed $x_{\Omega,i}$	(1) (2) (3) (4) $[0; 0.025) [0.025; 0.9) [0; 1) \ge 1 \times \Omega_{\text{gen}}^{\text{max}}$
valve pos. $u_{\mathrm{HSSV},i}$	$ \begin{array}{ccc} (1) & (2) & (3) \\ = 0 & [0.4; 1) & = 1 \end{array} $
elec. power $P_{\mathrm{elec},i}$	(1) (2) (3) ≤ -1 (-1; 1) ≥ 1 $\times P_{\text{gen}}^{\text{rated}}$
array motion moving RMS	$ \begin{array}{c cccc} (1) & (2) & (3) & (4) \\ [0;0.2) & [0.2;0.4) & [0.4;1) & \geq 1 \\ \end{array} $
battery charge $x_{\rm SOC}$	$ \begin{array}{c ccccc} (1) & (2) & (3) & (4) \\ [0;0.1) & [0.1;0.2) & [0.2;0.9) & [0.9;1) \\ \end{array} $

TABLE I Virtual Discrete Event Observer

Proposition 1. Fix a nonblocking Automaton G with closed language L(G) and marked language $L_m(G)$.

- 1) For nonempty $K \subseteq L(G)$ there exists a supervisor S such that L(G,S) = K iff K is prefix closed and controllable.
- 2) For nonempty $K \subseteq L_m(G)$ there exists a supervisor S such that $L_m(G,S)=K$, and the closed loop system is nonblocking iff K is controllable, and $\bar{K} \cap L_m(G)=K$

Further, K is controllable if

$$\bar{K}\Sigma_{\mathbf{u}} \cap L(G) \subseteq \bar{K}.$$
 (31)

Here, \bar{K} denotes a prefix of K. Therefore, (31) requires that any previous sequence of events in K, if followed by an uncontrollable event u, needs to be be a prefix of another sequence in K. This makes \bar{K} invariant under control action of $\Sigma_{\rm u}$. Clearly, due to the desired cyclic behavior of our designed supervisor D_i , this condition is satisfied. The Automaton G_i can always be pushed back into a sequence of events in K_i and furthermore, as the marked states are part of D_i , K_i is $L_{\rm m}(G_i)$ -closed, satisfying the second condition in proposition 1. Consequently, the supervisor can be realized with (T_i, ϕ_i) .

2) Virtual State Observer: The Automaton T_i , which is a component of the supervisor S_i functions similar to an observer. It uses the state space states, to detect the current discrete event state $q_i \in Q_i$. At this stage, knowledge about the system is incorporated into the numeric values that function as thresholds. The first three rows of Table I are taken for each WEC i, whereas the last two rows are global states. The extreme values originate from the physical constraints. The intermediate intervals for the rotational speed are determined from the efficiency of the generator shown in Fig. 2. It has to be noted that the value for the array motion which is based on the mean moving average root-mean-square (RMS) heave position of the three server WECs is somewhat arbitrary, but based on the observations of the time domain simulation model power generation capabilities.

3) Decision Maker: We use all five states detected in Table I to construct the state transition function ϕ_i for the supervisor S_i . We use a 5-tuple, with the respective dimension for the inputs, i.e. $\mathbb{Z}^{4\times 3\times 3\times 4\times 4}$ for every WEC i to implement a mapping from the instantaneous state q_i to a control action. The only difference between server and client array is that instead of activating c_{3S} , the supervisor will force the WECs in the server array to activate c_4 . The consequence of reaching a state with no predefined control action is c_9 , stopping the WEC.

IV. DYNAMIC SIMULATION

We conduct the time domain simulations with MATLAB-Simulink using the fixed time step Euler (ode1) solver because of the solver's reliability when handling discontinuous dynamics ($\Delta t=0.001\mathrm{s}$). To illustrate the effectiveness of the proposed control architecture, we use a highenergetic sea state, emulated by a random wave created with a Pierson–Moskowitz spectrum. We use a significant wave height $H_\mathrm{s}=4.5\mathrm{m}$ and peak period $T_\mathrm{p}=10\mathrm{s}$ over 1200s simulation time to go through different phases of WEC response. The detailed time evolution of important quantities from a client WEC (Nr.3) are illustrated in Fig. 5 as an example. For the discussion we are focusing on three time intervals, A, B and C.

- A: Power shedding. The supervisor activates the partial HSSV control multiple times to ensure the rotational speed stays between the $0.9\,\Omega_{\rm gen}^{\rm max}$ (dotted) and $\Omega_{\rm gen}^{\rm max}$ (dashed).
- B: More power is transmitted to the grid, since $x_{\rm SOC}$ is close to one. In the same interval, the reference following is briefly activated.
- C: Reference speed following. The server array has little motion response to the waves, thus the client WEC goes into the reference following SMC control. The peak-to-average power ratio decreases, but the electromagnetic energy conversion is forced to a higher efficiency.

V. CONCLUSION

We demonstrated a safe operation of WEC park, simulated in all DoFs, with a classical supervisory control approach that switches between ideal local controllers. We used power shedding based on more than just physical constraint, but also as a means of maintaining high efficiency. The proposed controller shows potential for further investigations with different local controllers, optimized for different operating regimes.

REFERENCES

- [1] J. Falnes, Ocean Waves and Oscillating Systems. Cambridge University Press, 2002.
- [2] D. García-Violini, N. Faedo, F. Jaramillo-Lopez, and J. V. Ringwood, "Simple controllers for wave energy devices compared," *Journal of Marine Science and Engineering*, vol. 8, no. 10, 2020. [Online]. Available: https://www.mdpi.com/2077-1312/8/10/793
- [3] J. V. Ringwood, "Wave energy control: status and perspectives 2020 **this paper is based upon work supported by science foundation ireland under grant no. 13/ia/1886 and grant no. 12/rc/2302 for the marine renewable ireland (marei) centre." IFAC-PapersOnLine, vol. 53, no. 2, pp. 12271–12282, 2020, 21th IFAC World Congress. [Online]. Available: https://www.sciencedirect.com/science/article/pii/S2405896320315536
- [4] T. K. A. Brekken, B. A. Batten, and E. A. Amon, "From blue to green [ask the experts]," *IEEE Control Systems Magazine*, vol. 31, no. 5, pp. 18–24, 2011.
- [5] J. Henriques, L. Gato, J. Lemos, R. Gomes, and A. Falcão, "Peak-power control of a grid-integrated oscillating water column wave energy converter," *Energy*, vol. 109, pp. 378–390, 2016. [Online]. Available: https://www.sciencedirect.com/science/article/pii/S0360544216305114
- [6] C. L. Oikonomou, R. P. Gomes, and L. M. Gato, "Unveiling the potential of using a spar-buoy oscillating-water-column wave energy converter for low-power standalone applications," *Applied Energy*, vol. 292, p. 116835, 2021. [Online]. Available: https://www.sciencedirect.com/science/article/pii/S0306261921003330
- [7] R. P. Gomes, L. M. Gato, J. C. Henriques, J. C. Portillo, B. D. Howey, K. M. Collins, M. R. Hann, and D. M. Greaves, "Compact floating wave energy converters arrays: Mooring loads and survivability through scale physical modelling," *Applied Energy*, vol. 280, p. 115982, 2020. [Online]. Available: https://www.sciencedirect.com/science/article/pii/S030626192031429X
- [8] P. Etxaniz, "Wave energy: An industry with a bright future," in *Bilbao Marine Energy Week*, 2017 [URL accessed on 2021-09-26]. [Online]. Available: https://www.bilbaomarinenergy.com/CMSPages/GetFile.aspx?guid=a8db6a1f-34f4-4548-a4e7-7f4dba46a76f
- [9] J. C. C. Henriques, W. Sheng, A. F. O. Falcão, and L. M. C. Gato, "A comparison of biradial and Wells air turbines on the Mutriku breakwater OWC wave power plant," in ASME 2017 36th International Conference on Ocean, Offshore and Arctic Engineering Volume 10: Ocean Renewable Energy, 06 2017.
- [10] P. C. Vicente, A. F. O. Falcão, and P. A. Justino, "A time domain analysis of arrays of floating point-absorber wave energy converters including the effect of nonlinear mooring forces," in 3rd International Conference on Ocean Energy, 2010.
- [11] A. I. Bratcu, I. Munteanu, D. C. Cernega, and M. Culea, "Safe and optimal operation of grid connected wind power systems by supervisory control," in EUROCON 2007 - The International Conference on "Computer as a Tool", 2007, pp. 2542–2549.
- [12] F. Fusco and J. V. Ringwood, "Hierarchical robust control of oscillating wave energy converters with uncertain dynamics," *IEEE Transactions on Sustainable Energy*, vol. 5, no. 3, pp. 958–966, 2014.
- [13] A. Wahyudie, M. Jama, T. Susilo, O. Saeed, C. Nandar, and K. Harib, "Simple bottom-up hierarchical control strategy for heaving wave energy converters," *Interna*tional Journal of Electrical Power & Energy Systems, vol. 87, 11 2016.
- [14] G. Giorgi, R. P. Gomes, J. C. Henriques, L. M. Gato, G. Bracco, and G. Mattiazzo, "Detecting parametric resonance in a floating oscillating water column device for wave energy conversion: Numerical simulations and validation with physical model tests," *Applied Energy*, vol. 276, p. 115421, 2020.

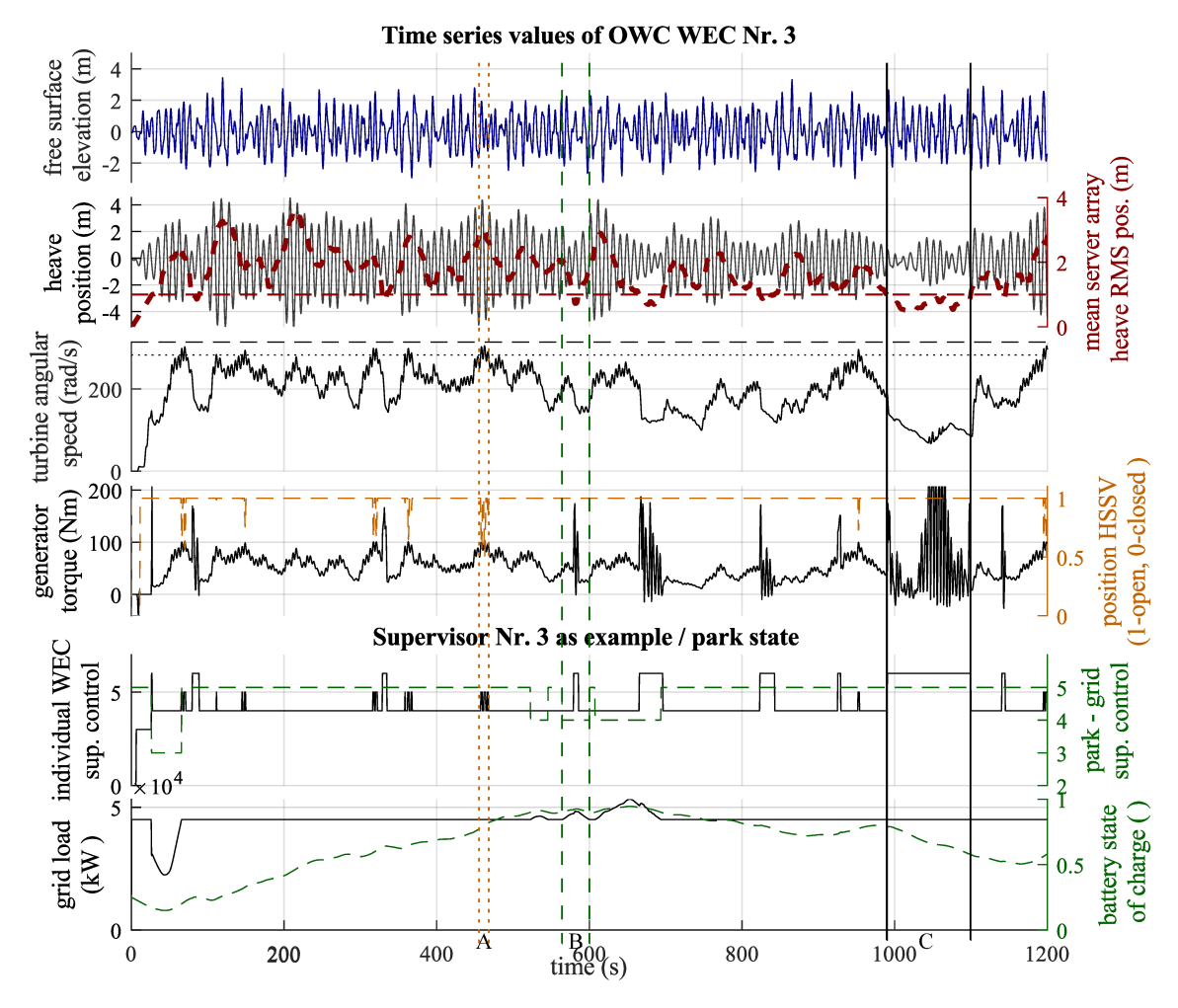


Fig. 5. Time series simulation results for the (client) WEC #3, in a random wave with $H_{\rm s}=4.5$ m and $T_{\rm p}=10$ s.

- [Online]. Available: https://www.sciencedirect.com/science/article/pii/S0306261920309338
- [15] D. T. Gaebele, M. E. Magaña, T. K. A. Brekken, and O. Sawodny, "State space model of an array of oscillating water column wave energy converters with interbody hydrodynamic coupling," *Ocean Engineering*, vol. 195, p. 106668, 2020.
- [16] C. Oikonomou, R. Gomes, L. Gato, and A. Falcão, "Analysis of a triangular array of floating oscillating water column devices with inter-body mooring connections in regular waves," in *Proc. 12th European Wave and Tidal Energy Conference*, 2017.
- [17] D. T. Gaebele, M. E. Magaña, T. K. A. Brekken, J. C. C. Henriques, A. A. D. Carrelhas, and L. M. C. Gato, "Second order sliding mode control of oscillating water column wave energy converters for power improvement," *IEEE Transactions on Sustainable Energy*, vol. 12, no. 2, pp. 1151–1160, 2021.
- [18] R. P. F. Gomes, "Wave energy extraction from oscillating systems: numerical modelling and experimental testing," Ph.D. dissertation, Instituto Superior Técnico, University of Lisbon, 2013.
- [19] S. A. Sirigu, M. Bonfanti, B. Passione, B. Ermina, B. Carlo, P. Dafnakis, G. Bracco, E. Giorcelli, and G. Mattiazzo, "Experimental investigation of the hydrodynamic performance of the iswec 1:20 scaled device," 2018.
- [20] A. A. D. Carrelhas, "Experimental study of the model and the prototype of a self-rectifying biradial air turbine with fixed guide-vanes. (in Portuguese)," Master Thesis, Instituto Superior Técnico, Universidade de Lisboa,

- 2017.
- [21] A. A. D. Carrelhas, L. M. C. Gato, J. C. C. Henriques, A. F. O. Falcão, and J. Varandas, "Test results of a 30 kW self-rectifying biradial air turbine-generator prototype," *Renewable and Sustainable Energy Reviews*, vol. 109, pp. 187–198, 2019.
- [22] P. J. G. Ramadge and W. M. Wonham, "The control of discrete event systems," *Proceedings of the IEEE*, vol. 77, no. 1, pp. 81–98, 1989.
- [23] J. Prosser, J. Selinsky, H. Kwatny, and M. Kam, "Supervisory control of electric power transmission networks," IEEE Transactions on Power Systems, vol. 10, no. 2, pp. 1104–1110, 1995.
- [24] J. C. C. Henriques, J. C. C. Portillo, W. Sheng, L. M. C. Gato, and A. F. O. Falcão, "Dynamics and control of air turbines in oscillating-water-column wave energy converters: Analyses and case study," *Renewable and Sustainable Energy Reviews*, vol. 112, pp. 571–589, June 2019.
- [25] K. D. Young, M. Thoma, and U. Ozguener, Variable Structure Systems, Sliding Mode and Nonlinear Control, 1st ed. Berlin, Heidelberg: Springer-Verlag, 1999.